### nature plants

**Brief Communication** 

https://doi.org/10.1038/s41477-023-01418-9

# Pavement cells distinguish touch from letting go

Received: 28 October 2022

Accepted: 14 April 2023

Published online: 15 May 2023

Check for updates

Alexander H. Howell<sup>1</sup>, Carsten Völkner<sup>1,2</sup>, Patrick McGreevy<sup>3</sup>, Kaare H. Jensen ® <sup>4</sup>, Rainer Waadt ® <sup>5</sup>, Simon Gilroy ® <sup>6</sup>, Hans-Henning Kunz ® <sup>1,2</sup>, Winfried S. Peters ® <sup>1,7</sup> & Michael Knoblauch ® <sup>1</sup> ⊠

A micro-cantilever technique applied to individual leaf epidermis cells of intact *Arabidopsis thaliana* and *Nicotiana tabacum* synthesizing genetically encoded calcium indicators (R-GECO1 and GCaMP3) revealed that compressive forces induced local calcium peaks that preceded delayed, slowly moving calcium waves. Releasing the force evoked significantly faster calcium waves. Slow waves were also triggered by increased turgor and fast waves by turgor drops in pressure probe tests. The distinct characteristics of the wave types suggest different underlying mechanisms and an ability of plants to distinguish touch from letting go.

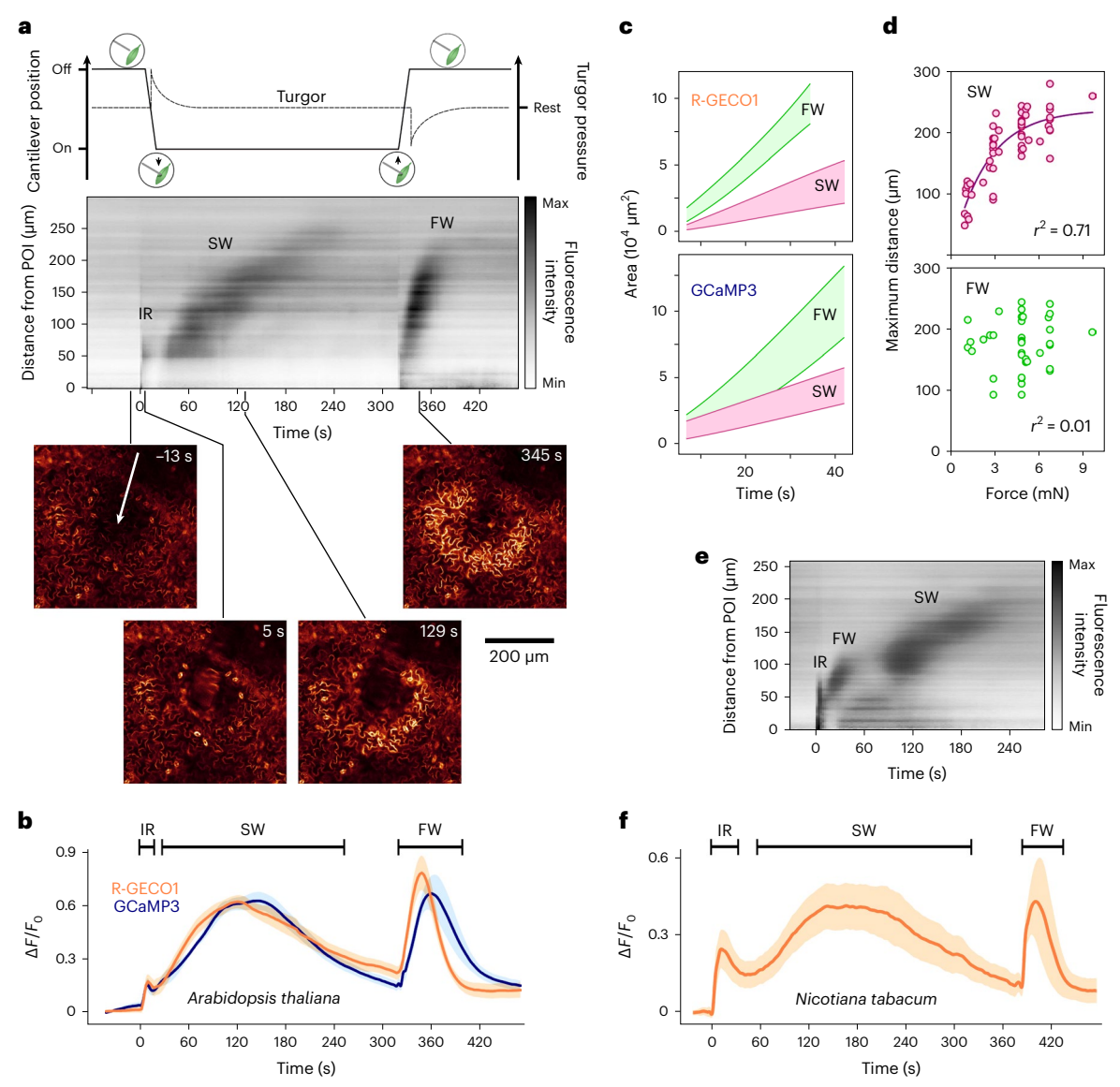
Mechanical stimulation affects plant growth and development<sup>1</sup>. Cytosolic calcium ([Ca<sup>2+</sup>]<sub>cvt</sub>) appears involved because mechanical stimuli often trigger [Ca<sup>2+</sup>]<sub>cvt</sub> transients<sup>2</sup> and enhance the expression of calmodulin-related genes<sup>3</sup>. The opening of Ca<sup>2+</sup>-permeable ion channels will allow Ca<sup>2+</sup> to move from organelles and/or apoplast into the cytosol<sup>4,5</sup>, and mechanosensitive Ca<sup>2+</sup> channels are well known from plants<sup>6-8</sup>. [Ca<sup>2+</sup>]<sub>cvt</sub> activates calmodulin, which then associates with calmodulin-binding transcription activators (CAMTAs) that bind to specific DNA motifs<sup>9,10</sup>. Promoters carrying CAMTA-binding motifs are overrepresented among touch-inducible genes<sup>11</sup>, suggesting that [Ca<sup>2+</sup>]<sub>cvt</sub> responses to mechanical stimuli affect gene expression via calmodulin and CAMTAs<sup>12</sup>. In *Arabidopsis* leaves, the mechano-induction of gene expression correlated with the zones covered by slow (~1 µm s<sup>-1</sup>) [Ca<sup>2+</sup>]<sub>cvt</sub> waves originating from mechanically stimulated, epidermal trichomes<sup>13</sup>, supporting the idea that trichomes act as mechanosensors<sup>14,15</sup>. However, numerous plant species are glabrous, and natural accessions of Arabidopsis vary from hairless to densely covered 16,17. To see whether epidermal cell types other than trichomes possess mechanosensory capabilities, we developed a micro-cantilever system that permits the reversible, non-invasive application of defined forces to individual pavement cells in intact plants under microscopic observation.

To study  $[Ca^{2^+}]_{cyt}$  responses to mechanostimulation in A. thaliana expressing the fluorescent calcium indicator R-GECO1 (ref. 18), intact plants were mounted on a confocal microscope stage so that

quantifiable forces could be applied to individual pavement cells in an abaxial leaf epidermis with micro-cantilevers (Supplementary Fig. 1). The responses were recorded, and  $[Ca^{2+}]_{cyt}$ -dependent fluorescence was analysed by averaging the fluorescence intensities of all pixels of the same distance from the point of impact in 1 µm steps; the mean intensities were plotted versus distance and time. In tests in which the cantilever rested on the cell for >3 min before being lifted off again, this approach identified three distinct responses (Fig. 1a).

In a set of 84 experiments conducted on 12 plants, an individual cell was subjected to a force of 0.1-12 mN. [Ca<sup>2+</sup>]<sub>cvt</sub> always increased immediately in that cell but dropped again within 10-15 s. This initial response (Fig. 1a,b) spread into an adjacent cell in only 8% of the tests. In all experiments, a wave of increased [Ca<sup>2+</sup>]<sub>cvt</sub> started to move radially from the point of impact at 20–50 s after stimulus application. This slow wave (Fig. 1a,b) dissipated after 3-5 min. In about half of the experiments, the removal of the cantilever at this time induced a [Ca<sup>2+</sup>]<sub>cvt</sub> wave that propagated visibly faster than the one induced by cantilever placement. This fast wave dissipated within 1 min (Fig. 1a,b). Similar responses were recorded in Arabidopsis synthesizing the alternative calcium sensor, GCaMP3 (Fig. 1b). The propagation of fast waves, quantified as the expansion of the circular area enclosed by the travelling fluorescence maximum, proceeded threefold faster than that of slow waves with both sensors (Fig. 1c). Using the longest distance from the point of impact at which a wave's maximum

<sup>1</sup>School of Biological Sciences, Washington State University, Pullman, WA, USA. <sup>2</sup>Department of Plant Biochemistry, Ludwig Maximilian Universität München, Planegg-Martinsried, Germany. <sup>3</sup>School of Electrical Engineering and Computer Science, Washington State University, Pullman, WA, USA. <sup>4</sup>Department of Physics, Technical University of Denmark, Lyngby, Denmark. <sup>5</sup>Institute of Plant Biology and Biotechnology, Westfälische Wilhelms-Universität Münster, Münster, Germany. <sup>6</sup>Department of Botany, University of Wisconsin–Madison, Madison, WI, USA. <sup>7</sup>Department of Biology, Purdue University Fort Wayne, Fort Wayne, IN, USA. ⊠e-mail: knoblauch@wsu.edu



stimulation in pavement cells of the *Arabidopsis* abaxial leaf epidermis. **a**, Standard experiment in which a defined compressive force was transiently applied to a leaf epidermis pavement cell by a micro-cantilever. Cantilever movements to and from the cell surface and the expected turgor shifts are outlined on top. In the middle, fluorescence intensities from a representative experiment (averaged for pixels of the same distance from the point of impact (position 0)) are plotted on a distance-versus-time field (cantilever placement was at 0 s, and removal was at 320 s). POI, point of impact; IR, initial response; SW, slow wave; FW, fast wave. Below, representative video frames are shown (Supplementary Video 1). **b**, Time courses of relative changes of  $[Ca^{2+}]_{cyt}$ -dependent fluorescence in a circle of radius 200  $\mu$ m around the cantilever's point

of impact (placement at 0 s, removal at 320 s) are similar for the two calcium

sensors, R-GECO1 and GCaMP3. The graphs represent means ± s.e. (R-GECO1:

n = 10, five biological replicates; GCaMP3: n = 6, three biological replicates;

Fig. 1 | Non-invasively evoked responses of cytosolic calcium to mechanical

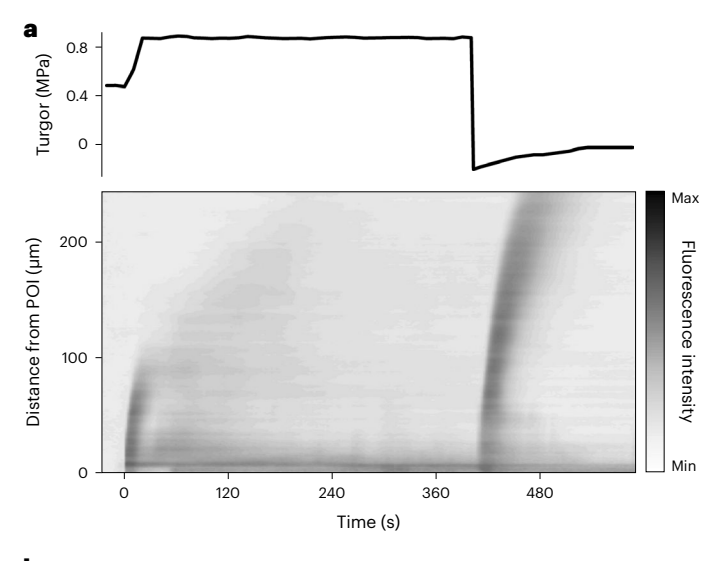
compare Supplementary Videos 1 and 2).  $\Delta F$ , change in fluorescence intensity;  $F_0$ , background intensity.  $\mathbf{c}$ , Wave propagation (expressed as the growth of the area within the expanding circle of maximal fluorescence) of slow and fast waves in wild-type Arabidopsis expressing R-GECO1 (top; n=10, five biological replicates) and GCaMP3 (bottom; n=7, three biological replicates). Each shaded area covers the mean  $\pm$  s.d.  $\mathbf{d}$ , Relationships between the force applied and the distance from the cantilever's point of impact to which slow waves (top; n=59) and fast waves (bottom; n=39) propagated before their maximum fluorescence intensity declined to <130% of the background level.  $\mathbf{e}$ , Experiment in which the removal of the cantilever 5 s after its placement (at time 0) triggered the initial response, fast wave and delayed slow wave simultaneously.  $\mathbf{f}$ , Responses to cantilever placement (0 s) and removal (380 s) in pavement cells of *Nicotiana tabacum* (R-GECO1: means  $\pm$  s.e., n=5, three biological replicates) resembled those in Arabidopsis (compare  $\mathbf{b}$ ; Supplementary Video 3).

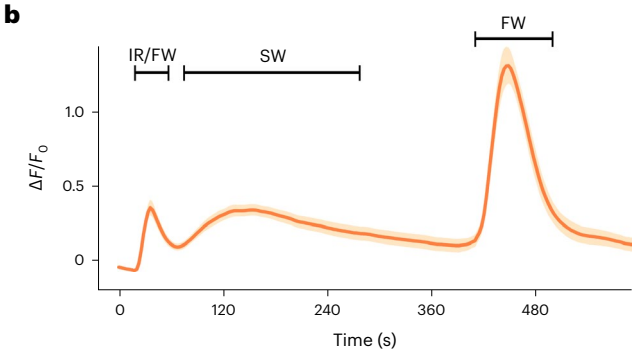
fluorescence intensity was  $\geq 30\%$  above background level as an estimate of propagation distance, we found the latter to correlate with applied force for slow but not for fast waves (Fig. 1d). As already noted, fast waves occurred in only a fraction of the experiments; their frequency tended to increase with increasing force (Supplementary Fig. 2). Interestingly, all three responses developed in parallel and overlapped in 14 of 57 experiments (25%; Fig. 1e) in which cantilevers were removed  $\leq 10$  s after touching a cell. In the remaining experiments, an initial

response occurred with either a slow wave (61%) or a fast wave (14%; Supplementary Fig. 3).

In *Nicotiana tabacum* expressing *R-GECO1*, abaxial leaf epidermis cells did not respond to forces under 8 mN. Greater forces triggered similar responses as in *Arabidopsis* (Fig. 1f).

Applying compressive forces to a cell increases intracellular pressure, and releasing them decreases it. To further elucidate the relationship between turgor shifts and  $[Ca^{2+}]_{cyt}$  responses, we manipulated





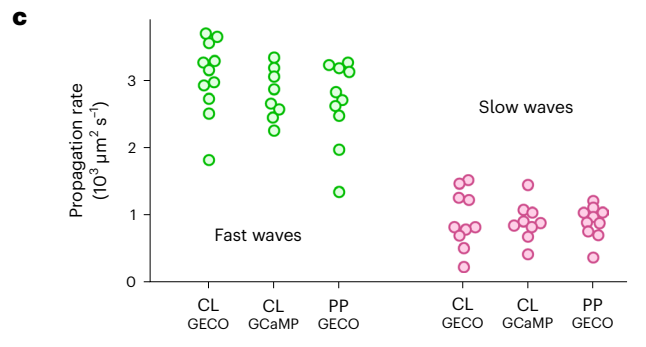


Fig. 2 | Invasively evoked cytosolic calcium responses to mechanostimulation in pavement cells of the abaxial *Arabidopsis* leaf epidermis, and comparison of propagation rates. a, Turgor in an individual cell was increased to 0.8 MPa after impalement (0 s) with a pressure probe and brought to ambient pressure 410 s later (compare Supplementary Video 4). Fluorescence intensities averaged for pixels of the same distance from the insertion (position 0) are plotted on a distance-versus-time field below the turgor graph. b, Relative changes of  $[Ca^{2+}]_{cyt}$  dependent fluorescence in a circle of radius 200  $\mu$ m around the insertion plotted versus time (means  $\pm$  s.e.; n = 10, five biological replicates). c, Propagation rates (velocities of the growth of the area within the circle of maximal fluorescence) of fast (left) and slow waves (right) averaged over the period from 20 to 30 s after the onset of the response. All individual measurements (7 < n < 12) are shown for waves induced by cantilevers (CL) and pressure probes (PP), with calcium sensor R-GECO1 or GCaMP3. Each fast-wave velocity differs significantly from each slowwave velocity ( $P \le 0.0001$ ; Student's t-test, two-tailed).

turgor with pressure probes in cells of Arabidopsis R-GECO1 plants. Impalement triggered a radial spread of  $[Ca^{2+}]_{cyt}$  that resembled early stages of fast waves (Fig. 2a,b). This wave faded when pressure was increased and maintained at a higher level, and a low-intensity slow wave developed instead (Fig. 2a,b). When fluorescence intensity had

returned to near resting level, pressure reduction always triggered a high-intensity fast wave (Fig. 2a,b). To compare waves triggered by different stimuli, we analysed the velocities of wave propagation averaged over a period when fast waves, the more rapidly dissipating type, showed particularly clearly (that is, from 20 to 30 s after the first sign of wave formation). The propagation rates of slow and fast waves induced by pressure probes were indistinguishable from those triggered by micro-cantilevers (Fig. 2c). This confirmed that slow waves were a response to turgor increases, whereas fast waves followed turgor drops.

When a cantilever touched a cell,  $[Ca^{2+}]_{\rm cyt}$  rose immediately but decreased again within seconds (IR in Fig. 1a,b). A cantilever obviously exerts a compressive force, which increases turgor pressure. The resulting disturbance of the cell's osmotic equilibrium drives water across the plasma membrane until equilibrium turgor is reestablished 19. Measured half-times of such turgor relaxations typically range around 10 s, but values <1 s are not unusual 20,21. The initial response thus coincided with water efflux and the consequent rise of intracellular osmolarity and drop of extracellular osmolarity that were induced by the mechanically evoked turgor increases (indicated in Fig. 1a, top). This alone does not prove causality, though. Cell wall deformation caused by the cantilever may also activate mechanosensitive  $Ca^{2+}$  channels independently of turgor pressure via increased membrane tension 22 or cytoskeletal force transmission 23.

The initial response to cantilever placement was followed by a slow [Ca<sup>2+</sup>]<sub>cvt</sub> wave with a delay of tens of seconds (SW in Fig. 1a,b). Evidently, the induction of slow waves required a time-consuming mechanism, and it seemed to encode quantitative stimulus features, as the distance travelled by slow waves correlated with the force applied (Fig. 1d). Slow waves also formed when turgor was elevated over extended periods with pressure probes (Fig. 2a,b), but not when cells were impaled without subsequent turgor increase (Supplementary Video 5). While turgor rises evidently were essential for eliciting slow waves, turgor increases probably relaxed within seconds in cantilever experiments as discussed above. The decisive factor evoking slow waves therefore might not be the turgor increase as such, but the resulting water efflux from the cell and the concomitant changes in intracellular and extracellular osmolarity. Observed half-times of hydrostatically induced turgor relaxations imply that water potential changes propagate at rates similar to that of diffusional mass flow<sup>20</sup>. A simple, plausible mechanism of slow-wave translocation could thus be based on the diffusive dissipation of disturbances of intracellular and/or extracellular osmolarity. Since the magnitude of the postulated osmolarity disturbance depends on the turgor shift induced and thus on the force applied, such a diffusive mechanism could account for the correlation between applied force and distance travelled by slow waves (Fig. 1d).

[Ca<sup>2+</sup>]<sub>cvt</sub> waves propagating significantly faster than slow waves (Fig. 2c) were always observed when turgor drops were induced by pressure probes (FW in Fig. 2a,b) and occurred in roughly half of the cantilever tests upon removal of the cantilever (Supplementary Fig. 2). Because these stimuli caused at least transient turgor decreases, the simplest hypothesis is that fast waves are triggered directly or indirectly by local turgor drops. However, the widths of the zones of elevated [Ca<sup>2+</sup>]<sub>cvt</sub> were often less than the dimensions of the pavement cells, and these zones appeared to move over the epidermis independently of cell boundaries (Supplementary Fig. 4). Turgor drops cannot be the immediate causes of such subcellular increases of  $[Ca^{2+}]_{cyt}$  when a fast wave passes, unless zones of substantially decreased turgor with diameters much below that of a cell moved slowly through individual cells. This seems physically impossible. Our observations could be explained by the release of a chemical signal, possibly an amino acid<sup>24</sup> or a reactive oxygen species<sup>25</sup>, into the apoplast where the wall and plasma membrane deform due to the removal of the cantilever, followed by diffusion of that signal in the apoplast. Where the chemical signal reaches a threshold concentration, it could activate mechanisms causing local rises in  $[Ca^{2+}]_{cyt}$ , such as  $Ca^{2+}$  channels. These mechanisms would soon have to turn inactive again, to account for the limited extension of the zone of elevated  $[Ca^{2+}]_{cyt}$ . In this scenario, the periclinal outer walls of the epidermal cells provide a planar layer in which signalling substances diffuse in all directions at similar velocities. This structural feature could explain the almost perfectly circular appearance of fast waves (Supplementary Videos 1, 2, 4 and 5).

Mechanically stimulated trichomes apparently initiate a single type of [Ca<sup>2+</sup>]<sub>cvt</sub> wave that correlates with effects on gene expression in surrounding cells13. Here we demonstrated mechanically induced [Ca<sup>2+</sup>]<sub>cvt</sub> waves in pavement cells, which may explain mechanical responsiveness in glabrous (that is, trichome-less) plants. In pavement cells, slow waves followed stimuli that increased turgor, while fast waves occurred when turgor dropped. The two wave types also differed in their lag phases after a stimulus, their propagation rates, the dependence of their propagation distances on the force applied and their lifetimes before dissipation. Moreover, overlapping slow and fast waves occurred in parallel under certain conditions (Fig. 1e and Supplementary Fig. 3). All this indicates distinct underlying mechanisms. To reveal how plants utilize the resulting potential to distinguish touch from letting go in a physiologically meaningful way, a reliable separation of the response types through carefully controlled force application procedures will be required in future studies. This will also facilitate the identification of mutants lacking one of the response types.

#### Methods

#### Plant material and growth conditions

Arabidopsis thaliana seeds were sown in soil (Professional Growing Mix, Sun Gro Horticulture) and stratified for 2 d at 4 °C prior to growing for 7 d in a growth chamber under short-day conditions (10 h light, 100  $\mu$ mol m<sup>-2</sup> s<sup>-1</sup> at 24 °C; 14 h darkness at 18 °C). Individual seedlings were transferred to custom-built pots suitable for microscopy and grown for another three weeks before experimenting. Arabidopsis UBQ10::R-GECO1 (ref. 26) and 35S::GCaMP3 (ref. 27) (a gift from K. Tanaka, Washington State University) were cultivated in the same way.

Nicotiana tabacum cv. Samsun was grown analogously but at 16 h light (25 °C)/8 h darkness (18 °C). Stable N. tabacum UBQ10::R-GECO1 transformants were generated by Agrobacterium-mediated transformation followed by tissue culture<sup>28</sup>. To design the reporter construct, R-GECO1 was amplified from genomic DNA of the A. thaliana sensor line using proofreading Phusion polymerase (New England Biolabs) and two oligonucleotides (forward, GTTTTTCTGATTAACAGACTAGT GATGGTCGACTCTTCACGT; reverse, CATCTTCATATGAGCTCCTAC CTACTTCGCTGTCA). Subsequently, the PCR product was inserted into a pG2.0::UBQ10::MCS::HSPterm HYG vector<sup>29</sup> by Gibson cloning (New England Biolabs). The reaction mix was heat-shock-transformed into Escherichia coli TOP10 chemically competent cells (Thermo Fisher). Correct resulting plasmids were selected on Kanamycin, prepped, sequenced and transformed into Agrobacterium strain GV3101 via electroporation.

#### Cantilever production and characterization

Borosilicate glass filaments were made from BR-100-10 glass rods (1.0 mm outer diameter; Sutter Instruments) using a Sutter model P-2000 micropipette puller. This process yielded two rods connected by a fine glass thread. Filaments with diameters of 50–100  $\mu$ m were cut from the thread and glued to an untreated glass rod with Loctite 352 (Henkel AG), a UV-curable resin. The tip of the filament was brought into contact with the heating coil of the puller to dull the edges.

Cantilevers of length L and diameter d were attached obliquely (in the vertical plane) to a micromotor that allowed vertical movement relative to a sample. When the cantilever tip contacted the sample, a force was exerted on the sample. For small deflections, force increases linearly with deflection h, according to linear beam theory<sup>30</sup>:

Force = 
$$\frac{3\pi}{64} \frac{d^4 E}{L^3} h$$

where E = 64 GPa is the elastic modulus of the cantilever and  $\pi d^4/64$  represents the moment of inertia for a solid cylindrical rod. We highlight four assumptions that underpin the linear beam model: (1) the load is applied at the tip, (2) the deflections are small relative to the beam diameter, and the beam is neither (3) displaced nor (4) deflected at the point of attachment. Finally, we assumed that the elastic modulus E of the borosilicate glass filaments is unaffected by the fabrication process.

To account for deviations from ideal beam theory, the system was calibrated using an AL1105 analytical scale (Ohaus). Cantilevers were lowered onto a plate until the force reading deviated from zero. Subsequently, the displacement h was increased in increments of 5  $\mu$ m from 0 to 50  $\mu$ m, in increments of 10  $\mu$ m from 50 to 100  $\mu$ m and in increments of 100  $\mu$ m from 100 to 1,000  $\mu$ m. Concurrently, force was monitored (Supplementary Fig. 5). The calibration confirmed the linear relation between h and force. However, to account for deviations from the ideal conditions in our experiments (1–4 listed above), we introduced a correction factor in the beam equation. On the basis of calibration experiments with individual cantilevers, this factor was always relatively close to unity, and the linear model could be applied within the limits of the calibration.

#### **Experimental procedures**

A pot with an individual Arabidopsis was placed sideways on the stage of a Leica TCS SP8 Confocal Laser-Scanning Microscope (Leica Microsystems). A petiole was carefully twisted so that the abaxial epidermis of a leaf of the intact plant, immobilized on the stage using double-sided carpet tape, could be monitored (Supplementary Fig. 1). Images were taken with a hybrid detector and a ×20 water-immersion lens (Leica Microsystems, objective no. 506147) at 512 × 512 resolution, scan speed 400 Hz, line averaging of 2 and pinhole set to 3 AU. R-GECO1 (excitation/emission, 561/580-620 nm) and GCaMP3 (excitation/emission, 488/500-550 nm) signals were recorded by time-lapse photography at 0.38 frames per second (2.6 s interval between images). Mounted plants were allowed to acclimate for 1 h. With the epidermis below the focal plane, the bottom edge of the cantilever tip was brought into focus (micromanipulator position zero). The cantilever was then lifted, and the epidermis was brought into focus. Before the cantilever was moved downwards to apply force, at least 25 frames (65 s) were collected to quantify the background fluorescence intensity,  $F_0$ .

For turgor manipulations of single cells, micropressure probes were prepared following standard procedures  $^{31}$ . Probes mounted on a custom-built pressure manifold were controlled by an MPC200 motorized micromanipulator (Sutter Instruments). The probes were pre-pressurized (0.4–0.5 MPa) before impalement.

#### Image processing and analysis

To analyse fluorescence intensities quantitatively in cantilever experiments, the x and y coordinates of the pixel where the cantilever touched the epidermis (the point of impact) were determined on 512 × 512 pixel micrographs using Image J (https://imagej.nih.gov/ij/). An algorithm was created to determine distances of pixels from the point of impact and averaging the intensities for pixels of the same distance in 1 μm steps (Supplementary Fig. 6 and https://github.com/patrickmcgreevy/geco\_data\_processing.git). The times at which the maximum fluorescence intensities were reached at different distances from the point of impact were established from the first derivative of B-spline interpolations using TableCurve2D (Systat Software). To determine the time courses of the velocities at which the fluorescence maxima moved, alternative regression models were fitted and ranked by the corrected Akaike information criterion<sup>32</sup>. For all datasets, two-parameter models provided the best fits. Wave propagation rates (dimension: area per unit time), defined as the velocity at which the area within

an expanding ring of maximum fluorescence intensity expands, were calculated from these models.

Overall fluorescence intensities within a 200  $\mu$ m radius around the point of impact were determined with the Leica LAS X software (Leica Microsystems). To quantify changes in fluorescence intensity,  $\Delta F$ , the difference between the intensity at a time and the background intensity  $F_0$  was divided by  $F_0$ .

#### **Reporting summary**

Further information on research design is available in the Nature Portfolio Reporting Summary linked to this article.

#### Data availability

Additional videos of calcium responses can be found at https://doi. org/10.5281/zenodo.6909354. Source data are provided with this paper.

#### Code availability

The algorithm created for determining average fluorescence intensities at defined distances from the point of impact is available at https://github.com/patrickmcgreevy/geco\_data\_processing.git.

#### References

- Coutand, C. Mechanosensing and thigmomorphogenesis, a physiological and biomechanical point of view. *Plant Sci.* 179, 168–182 (2010).
- Chehab, E. W., Eich, E. & Braam, J. Thigmomorphogenesis: a complex plant response to mechano-stimulation. J. Exp. Bot. 60, 43–56 (2009).
- Braam, J. & Davis, R. W. Rain-, wind-, and touch-induced expression of calmodulin and calmodulin-related genes in Arabidopsis. Cell 60, 357–364 (1990).
- Hamant, O. & Haswell, E. S. Life behind the wall: sensing mechanical cues in plants. BMC Biol. 15, 59 (2017).
- Landrein, B. & Ingram, G. Connected through the force: mechanical signals in plant development. J. Exp. Bot. 70, 3507–3519 (2019).
- Kurusu, T. et al. Plasma membrane protein OsMCA1 is involved in regulation of hypo-osmotic shock-induced Ca<sup>2+</sup> influx and modulates generation of reactive oxygen species in cultured rice cells. BMC Plant Biol. 12, 11 (2012).
- Yuan, F. et al. OSCA1 mediates osmotic-stress-evoked Ca<sup>2+</sup> increases vital for osmosensing in *Arabidopsis*. *Nature* 514, 367–371 (2014).
- Basu, D. & Haswell, E. S. The mechanosensitive ion channel MSL10 potentiates responses to cell swelling in *Arabidopsis* seedlings. *Curr. Biol.* 30, 2716–2728 (2020).
- Finkler, A., Ashery-Padan, R. & Fromm, H. CAMTAs: calmodulin-binding transcription activators from plants to human. FEBS Lett. 581, 3893–3898 (2007).
- Whalley, H. J. et al. Transcriptomic analysis reveals calcium regulation of specific promoter motifs in *Arabidopsis*. *Plant Cell* 23, 4079–4095 (2011).
- 11. Xu, Y. et al. Mitochondrial function modulates touch signalling in *Arabidopsis thaliana*. *Plant J.* **97**, 623–645 (2019).
- 12. Darwish, C. et al. Touch signaling and thigmomorphogenesis are regulated by complementary CAMTA3- and JA-dependent pathways. Sci. Adv. 8, eabm2091 (2022).
- Matsumura, M. et al. Mechanosensory trichome cells evoke a mechanical stimuli-induced immune response in *Arabidopsis* thaliana. Nat. Commun. 13, 1216 (2022).
- Liu, H. et al. Gradient mechanical properties facilitate Arabidopsis trichome as mechanosensor. ACS Appl. Mater. Interf. 8, 9755–9761 (2016).

- Zhou, L. H. et al. The Arabidopsis trichome is an active mechanosensory switch. Plant Cell Environ. 40, 611–621 (2017).
- Symonds, V. V. et al. Mapping quantitative trait loci in multiple populations of *Arabidopsis thaliana* identified natural allelic variation for trichome density. *Genetics* 169, 1649–1658 (2005).
- Sato, Y., Shimizu-Inatsugi, R., Yamazaki, M., Shimizu, K. K. & Nagano, A. J. Plant trichomes and a single gene *GLABRA1* contribute to insect community composition on field-grown *Arabidopsis thaliana*. *BMC Plant Biol.* 19, 163 (2019).
- Zhao, Y. et al. An expanded palette of genetically encoded Ca<sup>2+</sup> indicators. Science 333, 1888–1891 (2011).
- Wendler, S. & Zimmermann, U. Compartment analysis of plant cells by means of turgor pressure relaxation. II. Experimental results on Chara corallina. J. Membr. Biol. 85, 133–142 (1985).
- 20. Steudle, E. Water flow in plants and its coupling to other processes: an overview. *Methods Enzymol.* **174**, 183–225 (1989).
- Fricke, W. Water movement between epidermal cells of barley leaves—a symplastic connection? *Plant Cell Environ.* 23, 991–997 (2000).
- Hamilton, E. S., Schlegel, A. M. & Haswell, E. S. United in diversity: mechanosensitive ion channels in plants. *Annu. Rev. Plant Biol.* 66, 113–137 (2015).
- Tatsumi, H. et al. Mechanosensitive channels are activated by stress in the actin stress fibres, and could be involved in gravity sensing in plants. *Plant Biol.* 16, 18–22 (2014).
- 24. Bellandi, A. et al. Diffusion and bulk flow of amino acids mediate calcium waves in plants. *Sci. Adv.* **8**, eabo6693 (2022).
- 25. Johns, S., Hagihara, T., Toyota, M. & Gilroy, S. The fast and the furious: rapid long-range signaling in plants. *Plant Physiol.* **185**, 694–706 (2021).
- Waadt, R., Krebs, M., Kudla, J. & Schumacher, K. Multiparameter imaging of calcium and abscisic acid and high-resolution quantitative calcium measurements using R-GECO1-mTurquoise in *Arabidopsis*. N. Phytol. 216, 303–320 (2017).
- 27. Toyota, M. et al. Glutamate triggers long-distance, calcium-based plant defense signaling. *Science* **361**, 1112–1115 (2018).
- 28. An, G. High efficiency transformation of cultured tobacco cells. *Plant Physiol.* **79**, 568–570 (1985).
- 29. Pratt, A. I., Knoblauch, J. & Kunz, H. H. An updated pGREEN-based vector suite for cost-effective cloning in plant molecular biology. *microPubl. Biol.* **2020**, 000317 (2020).
- 30. Feynman, R. P., Leighton, R. B. & Sands, M. The Feynman Lectures on Physics: The New Millennium Edition—Mainly Electromagnetism and Matter Vol. 2 (Basic Books, 2011).
- 31. Tomos, A. D. & Leigh, R. A. The pressure probe: a versatile tool in plant cell physiology. *Annu. Rev. Plant Biol.* **50**, 447–472 (1999).
- 32. Motulsky, H. & Christopoulos, A. Fitting Models to Biological Data Using Linear and Nonlinear Regression (Oxford Univ. Press, 2004).

#### **Acknowledgements**

We thank V. V. Vasina for assistance with generating stable *Nicotiana tabacum pUBQ10::R-GECO1* transformants, M. Toyoda and K. Tanaka for sharing *35S::GCaMP3 Arabidopsis* seeds, S. Mühlbauer (LMU Munich) for help with figure design, and C. Cody and A. Linskey for plant care. Special thanks to D. L. Mullendore for troubleshooting and support. A.H.H. and C.V. acknowledge support from the Washington State University Elling and Higinbotham scholarship programme and a Washington State University Franceschi training grant. M.K. was funded by National Science Foundation (NSF) grant no. IOS-1656769. H.-H.K. was funded by an NSF Career Award (no. IOS-1553506), and S.G. was supported by NSF grant no. MCB2016177. We acknowledge technical support from the Franceschi Microscopy and Imaging Center at Washington State University, Pullman.

#### **Author contributions**

A.H.H., K.H.J., M.K., H.-H.K., W.S.P. and C.V. designed the experiments, and A.H.H. conducted the experiments. A.H.H. and C.V. generated the stable *Nicotiana tabacum* transformants. R.W. generated the stable *Arabidopsis thaliana pUBQ10::R-GECO1* plants. A.H.H., P.M., W.S.P. and C.V. analysed the primary data, and all authors discussed and interpreted the results. W.S.P. wrote the draft manuscript with input from A.H.H., H.-H.K. and C.V.; all authors discussed, augmented and improved the draft. M.K. coordinated the project.

#### **Competing interests**

The authors declare no competing interests.

#### **Additional information**

**Supplementary information** The online version contains supplementary material available at https://doi.org/10.1038/s41477-023-01418-9.

**Correspondence and requests for materials** should be addressed to Michael Knoblauch.

**Peer review information** *Nature Plants* thanks the anonymous reviewers for their contribution to the peer review of this work.

**Reprints and permissions information** is available at www.nature.com/reprints.

**Publisher's note** Springer Nature remains neutral with regard to jurisdictional claims in published maps and institutional affiliations.

Springer Nature or its licensor (e.g. a society or other partner) holds exclusive rights to this article under a publishing agreement with the author(s) or other rightsholder(s); author self-archiving of the accepted manuscript version of this article is solely governed by the terms of such publishing agreement and applicable law.

@ The Author(s), under exclusive licence to Springer Nature Limited 2023

# nature portfolio

Corresponding author(s):	Michael Knoblauch
Last updated by author(s):	Apr 8, 2023

# **Reporting Summary**

Nature Portfolio wishes to improve the reproducibility of the work that we publish. This form provides structure for consistency and transparency in reporting. For further information on Nature Portfolio policies, see our <u>Editorial Policies</u> and the <u>Editorial Policy Checklist</u>.

For all statistical analyses, confirm that the following items are present in the figure legend, table legend, main text, or Methods section.

$\overline{}$				
Š	+,	n t	 •+•	ics
٠,		71	 	

n/a	Confirmed
	$\square$ The exact sample size (n) for each experimental group/condition, given as a discrete number and unit of measurement
	A statement on whether measurements were taken from distinct samples or whether the same sample was measured repeatedly
	The statistical test(s) used AND whether they are one- or two-sided  Only common tests should be described solely by name; describe more complex techniques in the Methods section.
	A description of all covariates tested
$\boxtimes$	A description of any assumptions or corrections, such as tests of normality and adjustment for multiple comparisons
	A full description of the statistical parameters including central tendency (e.g. means) or other basic estimates (e.g. regression coefficient) AND variation (e.g. standard deviation) or associated estimates of uncertainty (e.g. confidence intervals)
	For null hypothesis testing, the test statistic (e.g. <i>F</i> , <i>t</i> , <i>r</i> ) with confidence intervals, effect sizes, degrees of freedom and <i>P</i> value noted <i>Give P values as exact values whenever suitable.</i>
$\boxtimes$	For Bayesian analysis, information on the choice of priors and Markov chain Monte Carlo settings
$\boxtimes$	For hierarchical and complex designs, identification of the appropriate level for tests and full reporting of outcomes
$\boxtimes$	Estimates of effect sizes (e.g. Cohen's <i>d</i> , Pearson's <i>r</i> ), indicating how they were calculated

Our web collection on statistics for biologists contains articles on many of the points above.

#### Software and code

Policy information about availability of computer code

Data collection

Primary data (digital confocal laser-scanning micrographs) were collected using the Leica LAS X v3.1.5 software (Leica Microsystems, Wetzlar, Germany) that comes as the standard software for controlling advanced Leica microscopes.

Data analysis

Original micrographs were processed with ImageJ v1.53, https://imagej.nih.gov/ij/. Overall fluorescence intensities in defined parts of the images were quantified with Leica LAS X v3.1.5 (Leica Microsystems, Wetzlar, Germany). MP4-versions of the supplementary videos were produced with QuickTimePro v7.7.9 (https://support.apple.com/downloads/quicktime). B-spline interpolations, numerical derivation, and regressions in the analysis of wave kinetics were performed with TableCurve2D (Systeat Software, San Jose CA, USA). The algorithm created for determining average fluorescence intensities at defined distances from the point of impact is available at https://github.com/patrickmcgreevy/geco\_data\_processing.git.References. Statistical tests (Student's t-tests) were performed using Vassarstats on vassarstats.net.

For manuscripts utilizing custom algorithms or software that are central to the research but not yet described in published literature, software must be made available to editors and reviewers. We strongly encourage code deposition in a community repository (e.g. GitHub). See the Nature Portfolio guidelines for submitting code & software for further information.

#### Data

Policy information about availability of data

All manuscripts must include a <u>data availability statement</u>. This statement should provide the following information, where applicable:

- Accession codes, unique identifiers, or web links for publicly available datasets
- A description of any restrictions on data availability
- For clinical datasets or third party data, please ensure that the statement adheres to our policy

All data used for producing the figures in the main paper are available in the 'Source\_Data' Excel file submitted. All data used for producing the Supplementary Figures are found in the 'Supplementary\_Data' Excel file that is included with the supplemental materials. Additional videos of calcium responses are available at https://doi.org/10.5281/zenodo.6909354.

#### Human research participants

Policy information about studies involving human research participants and Sex and Gender in Research.

Reporting on sex and gender	N/A
Population characteristics	N/A
Recruitment	N/A
Ethics oversight	N/A

Note that full information on the approval of the study protocol must also be provided in the manuscript.

# Field-specific reporting

Please select the one below that is the best fit for your research	. If you are not sure	, read the appropriate sectior	ns before making your selectior
--	-----------------------	--------------------------------	---------------------------------

🔀 Life sciences 💮 Behavioural & social sciences 🦳 Ecological, evolutionary & environmental sciences

For a reference copy of the document with all sections, see <a href="mailto:nature.com/documents/nr-reporting-summary-flat.pdf">nature.com/documents/nr-reporting-summary-flat.pdf</a>

## Life sciences study design

All studies must disclose on these points even when the disclosure is negative.

Sample size

No formal pre-determination of sample sizes was attempted because, first, the experiments initially had an exploratory character, and second, most comparisons were qualitative (e.g., "fast wave" present or not?). For the quantitative comparison of the propagation rates of slow and fast waves (Fig. 2c), we aimed at 8-10 independent repetitions for each treatment (different calcium sensors, cantilever or pressure-probe tests), and did not increase these sample sizes because statistical testing indicated that the two wave types differed at p<0.0001 for every treatment (compare Fig. 2c).

Data exclusions

Data (individual video files) were excluded only when technical issues, which unavoidably occurred in a fraction of the experiments (such as a spontaneous movement of the leaf out of the range in which the focal plane could be adjusted), made further analyses impossible.

Replication

All experiments were successfully repeated in multiple leaves (technical replicates) of several individual plants (biological replicates); the exact numbers of technical and biological replicates for each experiment reported are given in the figure legends and the main text.

Randomization

Plants for experiments were chosen randomly from large numbers of individuals cultivated together using the same equipment.

Blinding

Blinding was not performed. All plant lines used showed the same phenotype and thus were indistinguishable, and since the different results (slow wave only versus slow wave followed by fast wave) occurred in an essentially unpredictable manner in all plants, there was no possible experimenter's bias that could have been eliminated by blinding. Other comparisons analyzed in this study concerned potential differences between different fluorophores used and mechanostimulations applied (cantilever versus pressure-probe). It is impossible to conduct these experiments while blinded for the techniques used.

# Reporting for specific materials, systems and methods

We require information from authors about some types of materials, experimental systems and methods used in many studies. Here, indicate whether each material, system or method listed is relevant to your study. If you are not sure if a list item applies to your research, read the appropriate section before selecting a response.

# Materials & experimental systems Methods n/a Involved in the study n/a Involved in the study ☑ Antibodies ☑ ChIP-seq ☑ Eukaryotic cell lines ☑ Flow cytometry ☑ Palaeontology and archaeology ☑ MRI-based neuroimaging ☑ Animals and other organisms ☑ Clinical data

Dual use research of concern